High Performing Anion Exchange Membrane Water Electrolysis using Self-Supported Metal Phosphide Anode Catalysts and Ether Free Aromatic Polyelectrolyte

Sasidharan Sankar, [†] Roby Soni, [†] Hidenori Kuroki, [†] Shoji Miyanishi, [†] Takanori Tamaki, [†] Gopinathan M. Anilkumar, [†‡] Takeo Yamaguchi[†]*

[†]Laboratory for Chemistry and Life Science,
Tokyo Institute of Technology, R1-17, 4259 Nagatsuta, Midori-ku, Yokohama, Japan 226-8503
*E-mail: yamag@res.titech.ac.jp

[‡] R&D Centre, Noritake Co., Ltd., 300 Higashiyama,
Miyoshi-cho, Japan 470-0293

Abstract

Anion Exchange membrane water electrolysis (AEMWE) is going through the critical transition phase from laboratory scale to scale-up prospects owing to the development of highly durable ether-free aromatic anion exchange membranes. The next important step is processing competent nonprecious metal catalysts as scalable electrodes. Here, we fabricated an iron-integrated self-supported nickel phosphide (Ni_2P-Fe/NF) catalyst for the sluggish oxygen evolution reaction (OER). It was demonstrated that this catalyst could work as a high-performing anode electrode in an AEMWE system when combined with a durable ether-free aromatic polyelectrolyte. The noble metal-free Ni_2P-Fe/NF electrode developed employing a simple and scalable strategy demonstrated higher performance as an anode electrode in water electrolysis with a cell voltage of 1.73 V for 1 A/cm^2 with an excellent energy conversion efficiency (84%) in 1M KOH and is also found stable for 24 h at 200 mA/cm^2. Electrochemical and spectroscopic investigations over the Ni2P-Fe/NF metal electrode surface during & post-OER disclosed the beneficial synergistic interaction of the metal species leading to lattice alterations, formation of oxy-hydroxide active species, and improved electron charge transfer as crucial factors responsible for the excellent performance and stability. This work involving scalable processing of catalyst structures over nickel foam surface, insights into thickness variation of the substrate for catalyst ~~processing~~

1

~~and~~processing and identifying the OER characteristics under water electrolysis conditions are significant in the application direction of applying noble metal-free electrodes for green hydrogen generation in AEMWE.

Key Words: Anion Exchange Membrane Water Electrolysis, Green Hydrogen, Oxygen Evolution Reaction, Self-supported Catalysts, Metal Phosphide, Nickel Foam

TOC Graphic

$$4H_2O + 4e^- \rightarrow 2H_2 + 4OH^-$$

$$4OH^- \rightarrow O_2 + 2H_2O + 4e^-$$
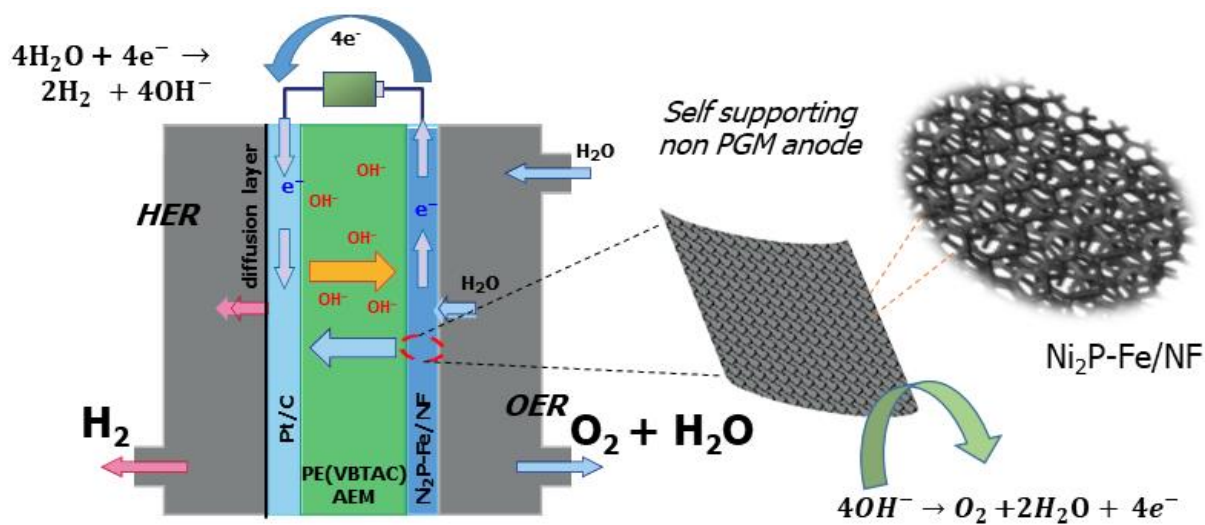
Nonprecious self-supported metal phosphide OER electrode for improved Anion Exchange Membrane Water Electrolysis performance and accelerating sustainable Green Hydrogen generation

Introduction

Green Hydrogen, derived from renewable resources, is an excellent energy carrier capable of meeting sustainable energy requirements.[1] A Hydrogen economy has immense potential to address the ever-growing global energy demands, with the advantages of being pollution free, clean, and sustainable, along with its high energy density of 142 MJ/kg.[2-3] Water electrolysis is a crucial technique and one of the most promising routes to yield green hydrogen involving the electrochemical splitting of water to form H2 and O2. However, it is a non-spontaneous process requiring high electrical energy to obtain significant amounts of H_2. For realizing water electrolysis, two major matured processes are often discussed; alkaline water electrolysis (AWE) and proton exchange membrane (polymer electrolyte membrane) based water electrolysis (PEM).[4-5] Although alkaline water electrolyzers have established merits, including low cost and higher durability,[6] AWE efficiency is typically low compared to PEM electrolysis and suffers from poor response to a fluctuating power supply.[7] PEMWE resolves these issues compared with AWE by using a thinner membrane in the application. In PEM electrolysis, however, the corrosive acidic environment and large overpotential for anodic water oxidation necessitate using precious metals as catalysts compared to AWE, where non-precious catalysts can be used. As such, despite having an efficiency advantage, the high-cost precious catalysts in acidic environments for PEMWE are always a significant limiting factor adding to the elevated cost of the system. This includes bipolar plates and current collectors using expensive precious metals such as Pt-coated titanium, accounting for ~68% of the total cost.

In this scenario, an alternative to PEMWE is the anion exchange membrane water electrolysis (AEMWE) involving alkaline electrolysis, where a thin anion exchange membrane (AEM) having lower OH⁻ transport resistance can be effectively utilized. In this system, where HER and OER

are the overall reactions, the diffusion of OH⁻ ions transpires through the AEM from the cathode to the anode, and electrons are being brought to the cathode through external circuit. Even though a fast growing concept for effective water electrolysis combining the benefits of PEM and AWE, AEMWE is still in the development phase and has been demonstrated mostly at the laboratory scale models with pursuit is on for improving performance focusing on different factors including diffusion layers.[8] With the AEM operating in an alkaline environment, the catalyst and current collector can be composed of inexpensive non-precious metals, which reduces the overall cost of the system and is a promising alternative to the matured technologies.[9] However, application of AEM to WE system is long limited due to poor durability of the membrane in alkaline circumstances. Recently, degradation mechanism of AEM in alkaline conditions was reported by several researchers[10,11] and several types of ether free aromatic polymers have been developed as durable AEMs to solve this degradation mechanism.[12-14] It has been demonstrated that some of these ether free AEMs show high performance and durability in AEMWE system.[15,16] Thus, the focus in AEMWE is gradually shifting towards developing and applying efficient, high performing non-precious metal-based catalysts that can be integrated with these high performing AEMs. As stated previously, alkaline water electrolysis operating in an alkaline environment does offer the window of using wider range of less expensive non precious metal catalysts.[17] However, it is still challenging to completely disregard the noble metals and replace them with alternative catalysts due to the lower mass activity and subsequent requirement of huge catalyst loadings.[18] As known, with the two half reactions occurring at anode and cathode, slower kinetics and high overpotential for oxygen evolution reaction (OER), caused by high energy requirements to break O–H is one of the major bottleneck in making the water splitting technology affordable and widespread.[19] Although many studies have been progressing for developing noble metal-free catalysts for water

splitting, their performance is far behind the Pt based (HER) and Ru/Ir based (OER) catalysts when assembled in the membrane–electrode-assembly (MEA) for anion exchange membrane water electrolyzers.[20-22] But, along with the scarcity and high cost in scaling up/integrating at commercial scale using noble metal catalysts, the dissolution and stability issues related have made it imperative to look for alternative earth abundant metal-based catalysts, and also improve strategies for diluting noble metals in catalyst compositions to be applied for MEA fabrication.[23] For alkaline water electrolysis, transition metal-based multimetal catalysts created using Ni, Co, Fe, etc., are increasingly sought lately, to amend the issues involving performance and cost effectiveness. These catalyst compositions being studied include phosphides, sulfides and nitrides, either unary or multimetal-based which are reported to be efficient and stable when compared with conventional catalysts.[24-30] Among them, transition metal phosphides (TMPs) are promising catalysts identified for both alkaline oxygen evolution (OER) and hydrogen evolution (HER) reactions, with excellent synergistic interactions among the constituents and phosphide acting as a layer to trap protons during HER.[31] Studies have also highly recommended that the construction of multi-metal phosphide compositions can create favorable electronic environment for water electrolysis.[32]

A further significant problem with catalyst processing and application when it comes to both commercial water electrolyzers including AEMWE and fuel cells is that the catalysts which shows good half-cell performance are mostly in powder state and need to be immobilized onto a current collector or membrane using a suitable polymeric binder.[33-34] The traditional fabrication method of electrodes for water electrolyzers involve a catalyst ink being generally spray-coated on the membrane, which is time-consuming and puts vast economic burden in the manufacturing process. This coating process, which is very important to maintain the catalyst stability and uniqueness,

increases the interfacial resistance between catalyst and membrane/current collector. In addition to this higher resistance, detachment of the catalysts and subsequent catalyst aggregation during long-term water electrolysis operations results in serious performance degradation of MEAs.[35-38] In this regard, developing of self-supported catalysts involving construction of catalyst layers or structures over 3D current collectors like nickel foam comes as a practical solution to overcome this problem while progressing in goal of realizing efficient and durable water electrolyzers. The identified advantages of these type of self-supported catalysts include direct use of catalysts as anode/cathode electrodes, excellent synergistic effect between the catalyst and substrate involved, reduced peeling off catalysts and more importantly superior charge transfer between catalyst layer and current collector.[39-40]

Thus, with the mandate of creating high performing nonprecious metal catalysts for AEM water electrolysis having stability and durability, we herein developed self-supported metal phosphide catalyst; iron-integrated nickel phosphide over nickel foam (Ni_2P-Fe/NF) using a simple and scalable two-step process (**Scheme 1a)**. Herein, we have used commercial porous nickel foam (NF) to prepare self-supporting metal catalyst structures and NF is a commonly used current collector in water electrolyzer systems due to its excellent electrical conductivity, low cost, good corrosion resistance in alkaline conditions and its high surface area.[41] Further, nickel foam current collector whose surface can be modified to act as a catalytically active surface should be an effective strategy to mitigate the cost of manufacturing and time during electrolyzer integration. The processed self-supported metal phosphide catalysts were tested initially in half-cell conditions for OER and then characterized in to identify the factors favoring excellent OER performance and stability. We then further testified these catalysts as anode electrodes by integrating MEA to create an excellently performing AEMWE, utilizing an in-house developed high molecular weight and

ether-linkage-free aromatic ionomer (poly- (fluorene-*alt*-tetrafluorophenylene) - trimethyl ammonium, PFT-C6-TMA) and a cross-linked poly (vinyl benzyl trimethyl ammonium chloride) (**PVBTAC**) pore-filling membrane filled in a porous polyethylene substrate: PE(VBTAC)) as the AEM. The schematic illustration of the developed membrane–electrode assembly (MEA) using the catalysts electrodes is shown in **Scheme 1b.** A very interesting aspect on the thickness of Ni_2P-Fe/NF electrodes were also carried out to understand the effect on AEMWE performances and to the best of our knowledge, electrolyzer tests for identifying the effect of self-standing anode electrode layer thickness on the water electrolysis performances is seldom reported.
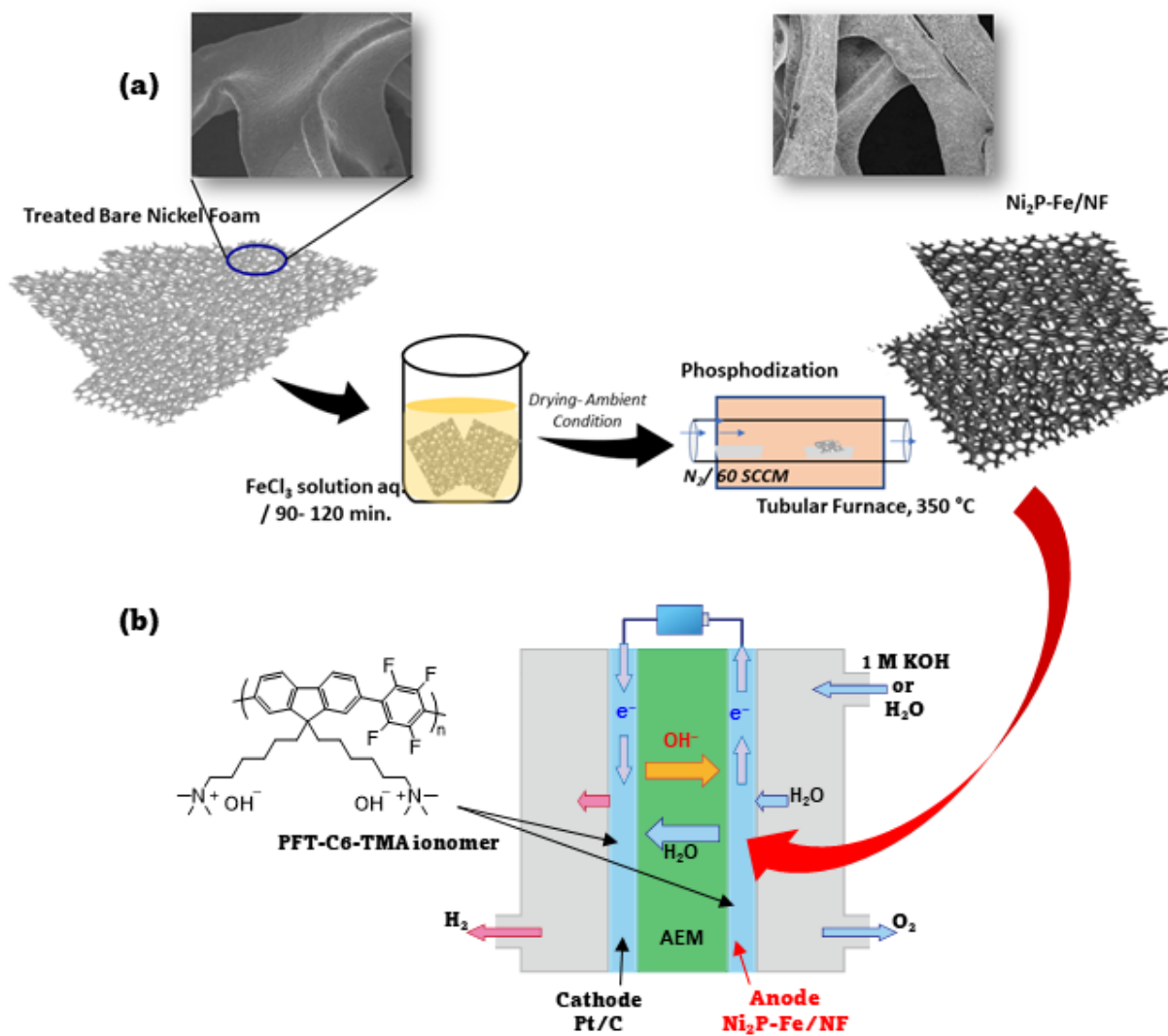
Scheme 1. (**a**) Illustration of the simple and scalable process for developing self-supported Fe integrated phosphide catalysts over nickel foam (Ni$_2$P-Fe/NF) and (**b**) the MEA system for AEM water electrolysis using the self-supported NF catalyst as Anode.

Results and Discussion

Structural characterization: The phosphide-based catalyst, Ni_2P-Fe/NF was prepared by initially dipping the mechanically pressed and surface treated NFs in aqueous iron precursor solution, followed by controlled heat treatment in the presence of phosphorous precursor under inert N_2 atmosphere (*see the experimental section for more details*). The processing of catalysts was carried out at varying thickness of NF, ranging from 220 µm to 800 µm and under varying phosphorization (2 – 6 h. at 2 h. intervals). The phase identification carried out using the X-ray diffraction (XRD) analysis indicated the formation of major Ni_2P phase in the surface and possible Ni_2P-Fe interaction over the NF substrate. **Fig 1a** shows the XRD patterns observed for the composition of the Ni_2P-Fe/NF catalyst and also depicts the XRD reference patterns of Ni_2P, Fe and Ni obtained from the International Centre for Diffraction Data (ICDD). The slight positive shift in 2θ for Ni for the Ni_2P-Fe/NF (**Fig 1b**) indicates a possible transformation in electronic environment for the Ni species on the surface, under the catalyst processing. This further shows an effective interaction facilitated among the metal species during the catalyst formation over the NF surface and the absence of Fe diffraction peaks in the XRD patterns points towards this prospect. **Fig 1c** and **Fig1d** are the structural representation of bare Ni foam and transformed NF to Ni_2P-Fe/NF(2h) during the processing. *Fig. S1* shows the X-ray diffraction patterns for the catalysts processed at longer phosphorization times (4 h and 6 h), indicate that the phosphide phase formed on the NF (220µm) surface was always similar. In the scanning electron microscopy (SEM) images for Ni_2P-Fe/NF, a uniform coverage of nanostructures over the NF could be seen (**Fig 1e, f**), stating the efficiency of the synthesis process for NF surface modification. *Fig. S3* shows the excellent adhesion of catalyst structures over the NF substrate which could prevent dissolution in OER conditions. Further, the energy dispersive spectroscopy (EDS) mapping of Ni_2P-Fe/NF (*Fig S2*) indicated an

undifferentiated distribution of Ni, P, Fe, O species throughout the surface of the NF and the SEM-EDS revealed ~3 wt.% of Fe and 20 wt.% of P content over the surface, which was supported by the ICP analysis. The overall catalyst loading varied in the range of 2-3 mg over the NF substrate.

Phase identification using X-ray diffraction was followed by X-ray photon spectroscopy (XPS) analysis and the deconvoluted spectrums for Ni $2p$, Fe $2p$ and P $2p$ binding energies in Ni_2P-Fe/NF(2h) are shown in **Fig 1g–i**. The XPS survey spectra for the modified NF catalyst showed Ni, Fe, P and O elements (*Fig S4*) confirming the successful modification. In the deconvoluted XPS spectra, Ni $2p$ region shows major binding energy peaks at 853.1 eV corresponding to Ni–P and 857 eV for Ni oxide (Ni–O) species (**Fig 1g**). There is also a smaller B.E. peak ascribed to $Ni(OH)_2$ on the surface at 861.2 eV with a satellite peak seen at 864.1 eV.[42-43] Interestingly, the partial positive charge associated with Ni species is noted from the Ni–P peak which is positively shifted and seen close to metallic Ni (852.7 eV) region.[44-45] In the case of Fe $2p$ (**Fig 1h**), two peaks are observed ascribed with major one for Fe $2p_{3/2}$ at 712.4 eV for oxidized (Fe–O) species and another B.E. peak at 706.1 eV for the interaction with P (Fe–P).[46-47] As could be understood from XRD, and the observed shift in XPS B.E. for Fe $2p$ supports the Fe doping in Ni lattice and bonding with P. When it comes to P species, peaks seen at 129.1 and 129.8 eV are connected P $2p_{3/2}$ with metal–P bond (Ni–P & Fe–P) and are at a negative shift compared to elemental P,[48-49] suggesting a partial negative charge as seen in **Fig 1i**. The positive shift of Ni $2p_{3/2}$ and negative shift of P $2p_{3/2}$ points at the altered electronic structure as observed from XRD and an enhanced electron transfer between Ni and P. The XPS peak at 134.2 eV binding energy corresponds to the oxidized species of PO_x with likely additional contribution from atmospheric exposure as well.[48,50]
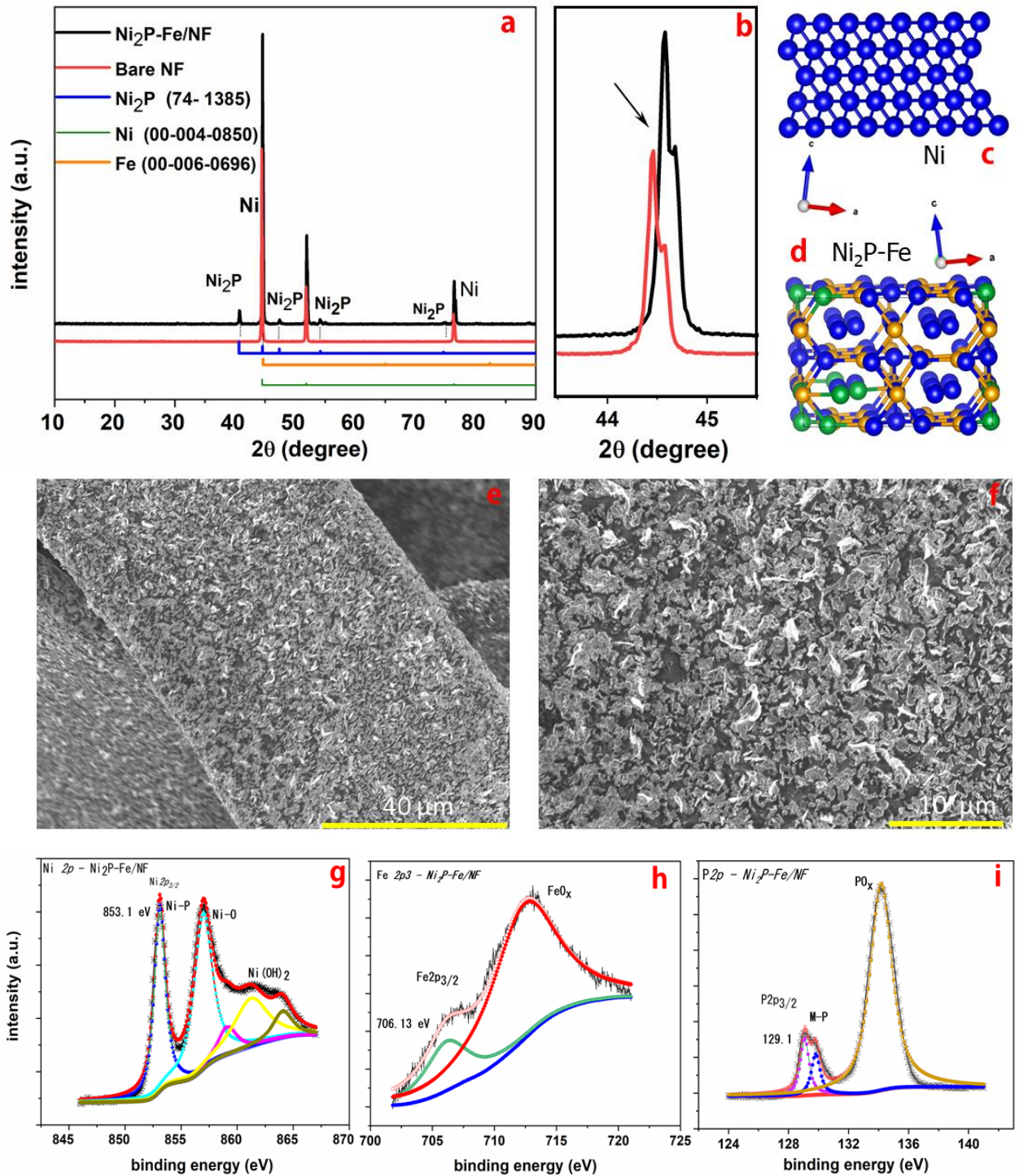
Figure 1. a) X-ray diffraction patterns of bare nickel foam and Ni_2P-Fe/NF (2h) with reference patterns observed for Ni_2P, Ni, Fe, **b)** deconvoluted X-ray patterns for Ni_2P-Fe/NF and bare NF showing the shift in 2θ **c-d)**schematic illustrations of Ni and Ni_2P-Fe/NF unit cells (*blue: Ni atom, yellow: P atom, green: Fe atom*) **e, f)** SEM micrographs of Ni_2P-Fe/NF showing the formation of nanostructured patterns over the NF surface, **g–i)** X-ray photon spectroscopy deconvoluted spectra

showing the oxidation states of Ni *2p* , Fe *2p* and P *2p* species respectively in the formed Ni_2P-Fe/NF catalyst.

Oxygen Evolution Performance: We conducted half cell (three-electrode cell) oxygen evolution reaction (OER) testing of Ni_2P-Fe/NF (*supplementary video*, **SV-1**), along with bare NF, and control NiFe/NF and Ni_2P/NF in N_2 saturated 1 M KOH aqueous solution. The solution IR compensated linear sweep voltammograms (LSV) recorded for OER are depicted in **Fig 2**. To avoid the interference of the Ni oxidation feature, we measured cathodic sweeps profiles of the different catalyst in which potential was scanned from high to low potential (*complete OER CV profiles are provided in Fig S6a*). The peak formed at around 1.3 V is due to the redox characteristics of the Ni based electrodes and also contribution from the introduction of Fe. In **Fig 2a**, initially processed Ni_2P-Fe/NF, which was prepared using NF with the thickness of 220 μm and a phosphorization time of 2 h, showed an overpotential of 210 mV (potential of 1.44 V) at the current density of 10 mA/cm^2, significantly lower than those of bare NF (350 mV), and Ni_2P/NF (270 mV) and control NiFe/NF (250 mV) samples. When the phosphorization time was increased during processing, OER performance of the phosphide catalyst varied and a further reduced OER overpotential of 185 mV was observed for 4 h (cathodic CV profiles shown in **Fig 2b**). However, the overpotential slightly increased on moving to 6 h phosphorization time similar to 2 h. A comparison of the overpotentials for Ni_2P-Fe/NF(4h) catalyst with recently reported nickel foam-based catalysts for OER in an alkaline electrolyte solution are shown in *Table S1*; which confirms that the Fe incorporated nickel phosphide catalysts showed outstanding efficiency during alkaline OER. Similar to the OER activity, the double layer capacitance (C_{dl})[47]also showed a marginal variation with the phosphorization times (*Fig S7b*), indicating higher electrochemically active sites at 4 h compared to other phosphorization times, causing the difference in OER performances. Tafel plots (**Fig 2c**) clearly demonstrated that Ni_2P-Fe/NF favors rapid OER kinetics with a Tafel slope

values of 14.4 mV/dec (Ni$_2$P-Fe/NF (2h)) and 12.6 mV/dec for Ni$_2$P-Fe/NF (4 h) at lower potentials, compared to Ni$_2$P/NF (30.6 mV/dec) and bare NF (46.1 mV/dec). The surface P content over the modified NF would activate water at lower potentials and thereby improving the resilience of the catalyst towards poisoning on the surface leading to improved activity,[51] as also could be seen from the Tafel slope values at low potentials. Further, the stability tests for Ni$_2$P-Fe/NF were carried out using the accelerated durability test (ADT) for 1000 CV cycles at 100 mV/s in the potential range of 1.3–1.6 V vs reversible hydrogen electrode (RHE) and the chronoamperometry (CA) test at 1.5 V vs RHE for 12 h. An improved OER performance (*Fig S9*) with lowered overpotential was observed. More importantly, detachment of metal constituents was observed below the detection limit from the ICP analysis of the electrolyte after the stability test indicating robustness of the catalyst surface in harsh conditions. Thus, the Ni$_2$P-Fe/NF (4h) is identified as the best catalyst composition with overall better OER performance under half cell conditions and was used for processing electrodes for further AEMWE studies.

After optimizing the annealing time (4h) and checking the OER performances followed by stability, we performed the alkaline OER analysis of Ni$_2$P-Fe/NF (4h) catalysts processed by varying the thickness of the NF substrate. Ni$_2$P-Fe/NF processed with the thickness of 220 and 400 µm showed virtually identical overpotentials for 10 mA/cm^2, while the thicker Ni$_2$P-Fe/NF catalyst with 800 µm in thickness showed an improved OER activity (**Fig 2d**) in half cell conditions as expected from higher difference in effective catalyst area. While analyzing the loading using ICP, there was also a slight increase in total loading of Fe and P constituents in the NF network for 800 µm sample also helping with a better OER performance in half cell conditions. The overpotential for achieving 100 mA/cm^2 was 230 mV for the Ni$_2$P-Fe/NF catalyst with 800 µm thickness and 250 mV for the catalyst with 400 µm compared to 270 mV for 200 µm. With C$_{dl}$ being considered

linearly proportional to ECSA, the electrochemically active surface area was estimated using the double layer capacitances and it suggested that higher thickness meant higher overall available catalyst area which could have helped with improved OER mass activity during half-cell electrolysis testing in 1 M KOH (aq.) The values obtained during C_{dl} measurement in mF/cm^2 is also normalized to the geometric surface area of NF, and the unit is [cm^2/cm$^2_{geo}$].
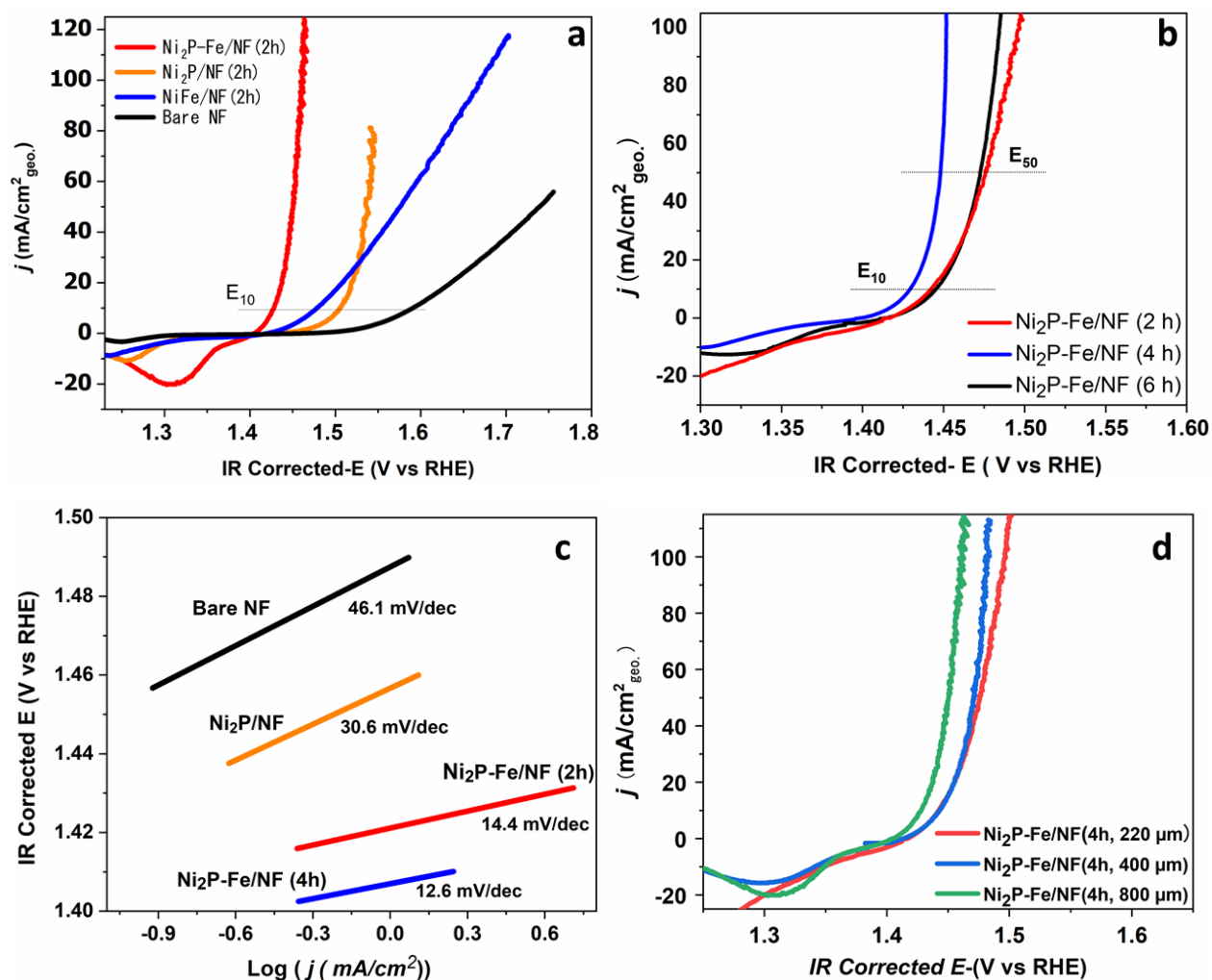

Figure 2. Oxygen evolution data using the developed self-supported catalysts in alkaline half-cell conditions: **a)** Cathodic CV profiles of the catalysts for OER at 10 mV/s in N$_2$ saturated 1 M KOH (aq.) **b)** Effect of varying phosphorization times on OER performance of the Ni$_2$P-Fe/NF **c)** Estimated Tafel slopes during OER for the catalysts at low potentials **d)** Impact on OER characteristics for Ni$_2$P-Fe/NF-4h during varying the thickness of NF (220–800 µm) while processing.

14

Analyzing the OER influencing factors: To develop highly active and efficient catalysts, it is essential to identify the originating factors for the excellent performance of the developed catalysts. To begin with, initially we analyzed the increase in OER actives sites by the formation of phosphide phase and Fe incorporation by calculating the ECSA from double layer capacitance (C_{dl}) for different catalysts (*Fig S10a-d*). The C_{dl} was calculated from the slope of the plots (*Fig S10d*), drawn after averaging the differences in anodic and cathodic part at different scan rates. The bare NF (220 µm) gave an estimated ECSA of 2.1 cm^2/cm_{geo}^2 while Ni_2P/NF (2h, 220 µm) showed a value of 2.4 cm^2/cm_{geo}^2 and Ni_2P-Fe/NF (2h, 220 µm) displayed an ECSA value of 3.8 cm^2/cm_{geo}^2. The effective increase in ECSA for Ni_2P-Fe/NF could be attributed to the successful interaction of introduced Fe, P species with Ni surface and improved charge transfer benefits. A lower charge transfer resistance for the Ni_2P-Fe/NF from the electrochemical impedance analysis (EIS) (*Fig. S11a*) compared to bare NF and also Ni_2P/Fe at 1.5 V vs RHE indicated a faster OER kinetics being favored by Fe and P incorporations. Further, the EIS measurements for the different phosphorization times also indicated the better charge transfer benefits for the Ni_2P-Fe/NF catalysts (*Fig. S11b*). More active sites from incorporation of Fe in Ni/Ni_2P system would be one of the reasons for the excellent OER activity of Ni_2P-Fe/NF. Further, the Ni_2P-Fe/NF catalyst exhibited much lower Tafel slope values at low potentials than those of the bare NF and Ni_2P/NF catalyst, implying faster OER kinetics due to the beneficial surface modification

After understanding the electrode characteristics in terms of surface area and favorable charge transfer kinetics from the processing of Ni_2P-Fe/NF catalysts, effects of Fe, P and their oxidation characteristics in OER kinetics are to be discussed. The incorporation of Fe would act favorably to improve the redox activity of Ni surfaces by lower oxygen adsorption activation energy.[52-53] Fe in Ni_2P-Fe/NF also would show a synergistic interaction to create the favorable electronic structure

of Ni in Ni_2P by forming Fe $3d$ state at fermi level. Further, since nickel oxy-hydroxides are known for strong interaction with Fe,[54] the incorporation of Fe boosts the formation of oxy-hydroxide phases of Ni, which are highly active phases for OER in alkaline conditions. As reported previously, it is understood that the interaction between oxy/hydroxide species of nickel and PO_x species are beneficial for OER. [55-56] For understanding the characteristics of the metal species in the NF catalyst surface under varying electrolyzer conditions, a detailed analysis was carried out after electrolyzer MEA studies and results are provided in the upcoming session.

Anion Exchange Membrane Water Electrolysis:

After the OER half-cell analysis and identifying the ECSA accessible with different modifications for the catalysts, we assessed the utility of the best prepared NF-based catalysts as self-supported anode electrodes in the AEMWE cell. After the OER half-cell analysis and identifying the ECSA accessible with different modifications for the catalysts, we fabricated MEAs with durable ether free poly(fluorene-*alt*-tetrafluorenephenylene) ionomer to assess the utility of the best prepared NF-based catalysts as self-supported anode electrodes in the AEMWE cell. For the AEM of the MEAs, PVBTAC membrane filled in the porous polyethylene substrate was used (AEM fabrication is explained in the experimental section). To enhance the chemical durability of the membrane, thin poly(fluorene-*alt*-tetrafluorenephenylene) polyelectrolyte layer was coated on the surface of the membrane by a simple dip coating to protect PVBTAC from the attack of OH- anion. The coated AEI layer is also beneficial to construct better electrochemical contact with the catalyst layer and the poly(fluorene-*alt*-tetrafluorenephenylene) ionomer.

For the initial study, the best performing Ni_2P-Fe/NF catalyst (phosphorization time = 4 h, thickness = 220 µm) and the bare NF catalyst (thickness = 220 µm) were used. The polarization curves for the AEMWE obtained at 80 °C using 1 M KOH (aq.) fed to the anodes are provided in

Fig 3a. The MEA with the Ni_2P-Fe/NF catalyst at the anode yielded a current density of 1 A/cm^2 at a low cell voltage of 1.73 V and 2 A/cm^2 at 1.9 V. The energy conversion efficiency calculated using the thermo-neutral voltage of 1.48 V were 86% and 78% at 1 and 2 A/cm^2, respectively. The MEA with the bare NF catalyst at the anode showed 2.1 and 2.3 V at 1 and 2 A/cm^2, respectively. Thus, the efficient OER catalyst of Ni_2P-Fe/NF provided the much higher AEMWE cell performances, compared with bare NF. To effectively compare the catalyst performance with commercial catalysts, the MEA with IrO_2 anode was also fabricated. As shown in **Fig. 3a**, the polarization curve of the MEA with the IrO_2 anode indicates a cell voltage of 1.77 V and 1.97 V at 1 and 2 A/cm^2, respectively, whose performance was lower than the MEA with the Ni_2P-Fe/NF anode. These results indicate the Ni_2P-Fe/NF (4 h,220 µm) catalyst can be an effective substitute for expensive commercial IrO_2 as a high-performance anode electrode in AEMWE. The stability of the Ni_2P-Fe/NF catalyst during the AEMWE operation was also evaluated. When the cell with Ni_2P-Fe/NF anode was subjected to operation at a constant current density of 200 mA/cm^2 and 80 °C using 1 M KOH feed, the cell voltage showed no deterioration in performance for 24 h (**Fig 3b**), indicating the performance stability of the electrolyzer cell. ICP-MS analysis of the electrolyte after the CA test also showed no degradation of metallic constituents.
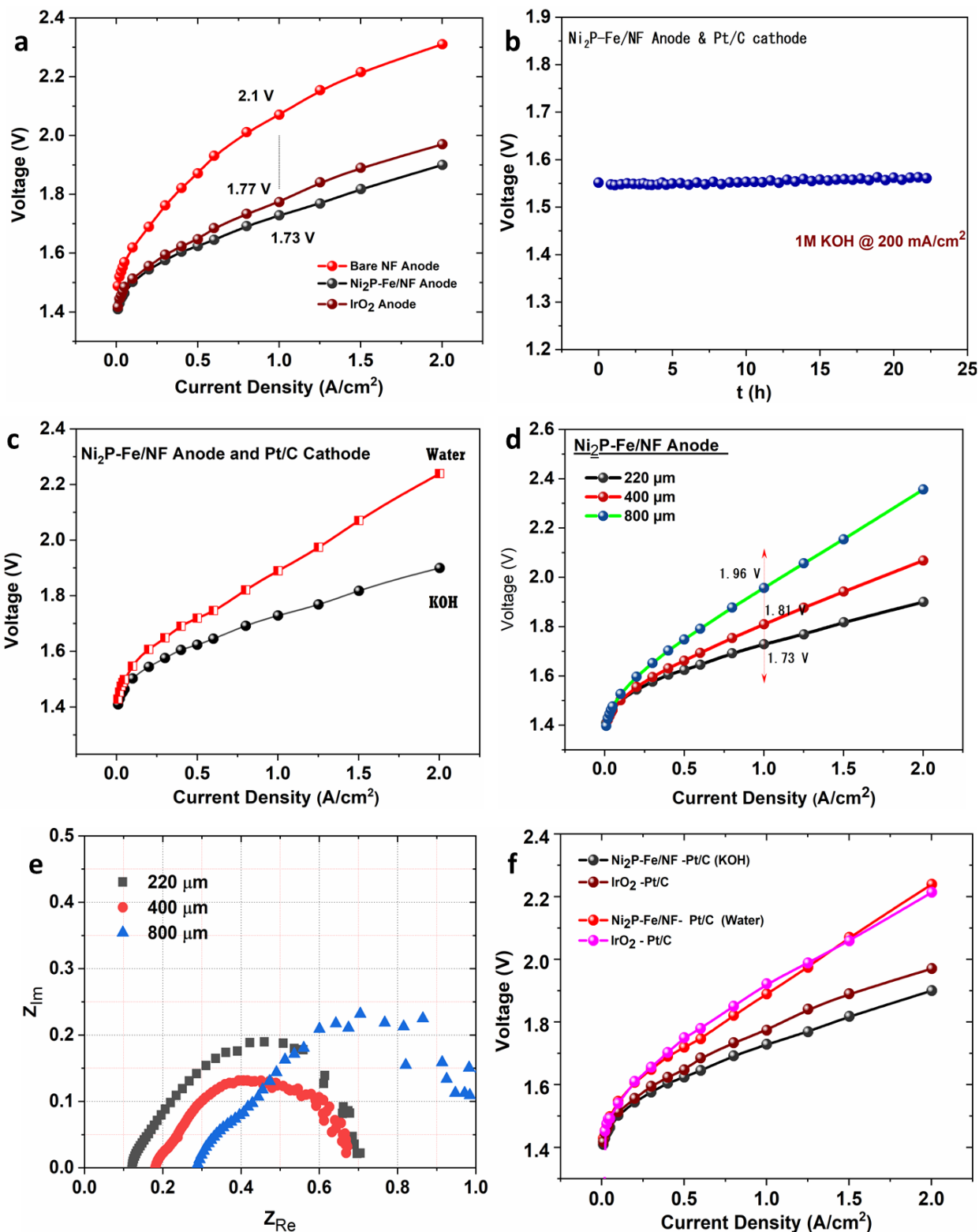
Figure 3. AEMWE performances utilizing the self-supporting Ni₂P-Fe/NF catalysts at the operation temperature of 80 °C **a)** Polarization curves using 1 M KOH aq. for the electrolyzer with bare NF, Ni₂P-Fe/NF, and commercial IrO₂ as the anodes and Pt/C as the cathode **c)** Polarization curves in pure water and 1M KOH feed for Ni₂P-Fe/NF – Pt/C system employing PFT-C6-TMA

ionomer **d)** Electrolyzer performances for electrolyzer while varying the Ni_2P-Fe/NF catalyst electrode thickness **e)** EIS spectra for the Ni_2P-Fe/NF with varying thickness in 1 M KOH.

Furthermore, the Ni_2P-Fe/NF anode electrode was tested in pure water flow and this electrolyzer (as shown in **Fig. 3c)** exhibited excellent efficiency with a cell voltage of 1.88 V at 1 A/cm^2 (energy conversion efficiency = 79%). This high performance in pure water feed was largely due to the high OH$^-$ conductivity of the ionomer and the AEM, but it was demonstrated that non-precious Ni_2P-Fe/NF catalysts can achieve the high performance of pure-water-fed AEMWE if properly integrated with electrolyte materials. The comparison of the AEMWE performances (alkaline and pure water feed) with the MEAs using non-PGM anodes as reported recently is shown in *Table S3.* From **Table S3**, it can be concluded that our MEA with the Ni_2P-Fe/NF catalyst is one of the MEAs showing high AEMWE performances. Nevertheless, more recently few papers have reported the MEAs with higher AEMWE performances than our MEA, suggesting that optimization of an MEA, including ionomer and AEM to be combined with a Ni_2P-Fe/NF catalyst, is necessary.

After the excellent performance of the electrodes under electrolyzer conditions, we continued AEMWE cell testing by varying the thickness of the NF (Ni_2P-Fe/NF) electrodes (220–800 µm). **Fig 3d** shows the polarization curves for the AEMWE results obtained with Ni_2P-Fe/NF as anode of processed over NF thicknesses 220, 400, and 800 µm in 1 M KOH (aq.). MEA with anode of lowest thickness, i.e., 220 µm showed best performance reaching 1 A/cm^2 current density at 1.73 V whereas electrolyzer with anode thickness 400, 800 µm required 1.81 and 1.96 V, respectively, to attain similar current density. This increase in cell voltage with thickness is attributed mostly to the increased cell resistance for the MEAs, as evident from the electrochemical impedance analysis (**Fig 3e**). The Tafel plot for the MEA polarization curves (*Fig S12a*) with varying thickness of

Ni$_2$P-Fe/NF showed a higher mass transfer resistance while using the thicker electrode (152.8 mV/dec for MEA having 800 µm Ni$_2$P-Fe/NF compared to 104.4 mV/dec for MEA with 220 µm Ni$_2$P-Fe/NF). Similarly, for the polarization curves during electrolysis in pure water feed with Ni$_2$P-Fe/NF – 400 and Ni$_2$P-Fe/NF – 800 reached 1.93 V and 2.22 V at 1 A/cm^2 current density, respectively, showing the tendency of thicker electrode to require high energy for water splitting (*Fig S12b*).Thus, the self-supported Ni$_2$P-Fe/NF (4 h,220 µm) is identified as the ideal anode for AEMWE in the present study, which can be an important reference for future AEMWE design and commercialization purposes utilizing self-supported catalysts including based on nickel foam. The Ni$_2$P-Fe/NF anode electrode used for CA studies in AEMWE condition was tested in detail for evaluating the surface characteristics and insights into the performance factors.

Ni$_2$P-Fe/NF electrode surface assessment after MEA testing: The SEM analysis of the electrodes taken after the water electrolysis followed by the constant current durability test showed the formation a thin layer over the surface and while analyzing with energy dispersive spectroscopy (EDS), an enhanced oxygen distribution was noticed (*Fig S13*). Then we carried out the XPS analysis of the electrode surface and when we examined the deconvoluted spectra, the Ni *2P* peak at 856.2 eV (**Fig 4a**) indicated oxide phased M–P species and the peak observed at 861.8 eV indicated the formation of Ni (OH)$_2$ phase.[48,57] Thus, the OER active phase of oxide/oxy-hydroxide formation over the Ni$_2$P-Fe/NF electrode surface is confirmed during the water electrolysis, which favors the stable oxygen evolution performance in alkaline conditions.

The peaks associated with M–P species in the pristine Ni$_2$P-Fe/NF electrode were converted completely into PO$_x$ state, which could be characteristic of tetrahedral PO$_x$ group, according to the peak for P*2p* species seen at ~133.6 eV (*Fig S14a*) with a reduction in intensity.[50,58] The formation of oxidized P species could be further confirmed by the O *1s* peak at 533.2 eV (*Fig S14b*). As

discussed previously, the successful interaction between formed oxy/hydroxide species of nickel and PO_x would act as a ligand and vary its coordination modes during the redox swapping process of the metal ion and further, the presence of these phosphates would also facilitate the electron/proton transfer, enhancing the OER kinetics and help in overall improved electrolyzer performance. On analyzing the Fe *2p* species, the peak at 706 eV had disappeared and the peaks are seen at a lower intensity after being oxidized at 712.6 and 718.7 eV post OER (**Fig 4b**). Thus, an atomic-level surface reconstruction of the modified Ni_2P-Fe was observed after the stability test and these changes are supportive for enhanced OER activity. The surface reconstruction was successfully established further when the XRD analysis of the anode electrode showed the peaks associated with oxide species of metals (*Fig S15*) after the CA test. Hence, it can be explicitly inferred that the metal-oxide/hydroxide species would act as the major active sites in the processed Ni_2P-Fe/NF, which further facilitated the electron transfer from metal species to the oxidized species, for providing dynamically stable OER under alkaline conditions.[59-60]
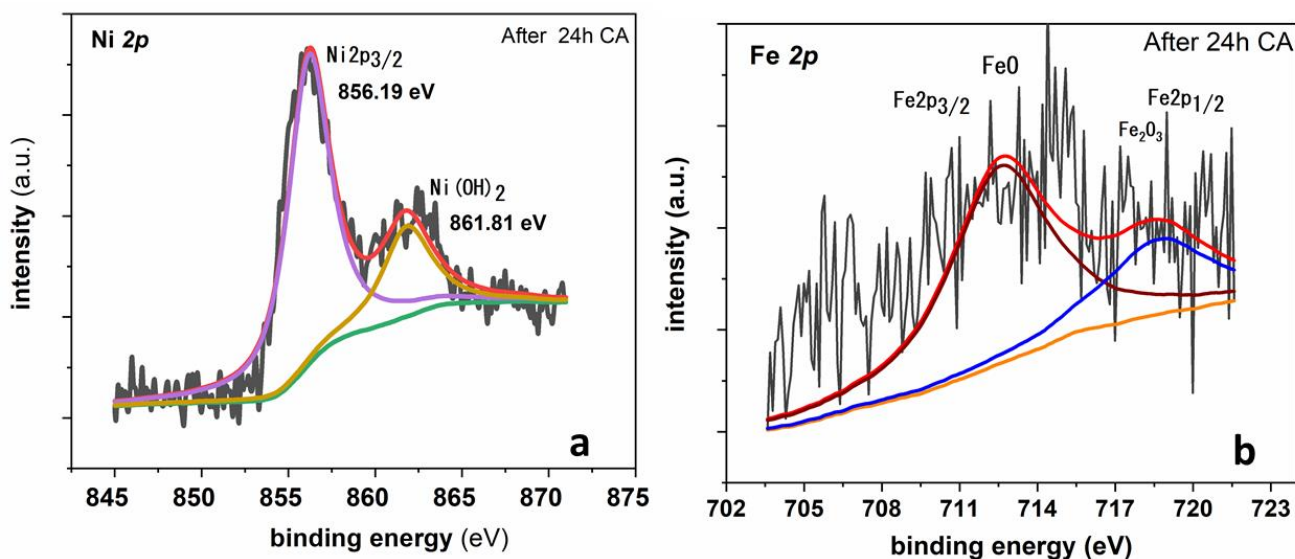

Figure 4. Deconvoluted XPS spectra for **a)** Ni *2p* and **b)** Fe *2p* after 24 h stability tests in the water electrolyzer for Ni_2P-Fe NF at 200 mA/cm^2

From the excellent MEA test results in water electrolysis, the self-supported Ni_2P-Fe NF catalysts developed using our simple and scalable approach is testified as an excellent electrode material for AEM-based water electrolysis; with the developed system performing at par with commercial catalysts which signifies its tremendous commercial potential and further development. The catalysts also showed excellent stability with no detachment during long term stability studies which are extremely advantageous over currently used powder catalysts by virtues of its application ease and excellent performance. With many parameters involved in electrolyzer integration including catalysts, ionomers, AEM membrane type and thickness, we are currently involved in navigating strategies to improve further with AEM electrolyzers using the nickel foam based self-supported catalysts.

Conclusions

In this study, scalable self-supported non-noble metal electrodes favoring excellent oxygen evolution reaction performance in AEMWE were developed and demonstrated. The OER catalyst, Ni_2P-Fe/NF was obtained over nickel foam using Fe as the multi-metal constituent which were phosphodized under controlled conditions. The catalyst under half cell conditions yielded 10 mA/cm^2 current at 185 mV overpotential for OER in 1 M KOH electrolyte solution and displayed excellent stability in accelerated conditions. The MEA using the Ni_2P-Fe/NF catalyst at the anode for AEMWE using 1 M KOH aq. generated sufficiently high performance achieving 1 A/cm^2 current density at 1.73 V with an excellent energy conversion efficiency (84%). Also, the combination of the Ni_2P-Fe/NF catalyst, highly conductive inhouse ionomer (PFT-C6-TMA) and a pore filled VBTAC AEM with thin PFT-C6-TMA layer achieved an excellent pure-water-fed AEMWE performance delivering 1 A/cm^2 at 1.88 V. Furthermore, in this study, we could study a critical factor for water electrolyzers using self-supported catalysts involving the thickness of self-

supported catalyst electrodes. With the thickness for NF based catalysts being varied from 220–800 µm, the cell resistance increased with thickness and the performance dropped for the AEMWEs in both alkaline and pure water fed conditions. In addition to the excellent water splitting performance of Ni_2P-Fe/NF in half-cell and MEA testing, our study also successfully demonstrated the factors responsible for the excellent OER performance by means of comprehensive spectroscopic and electrochemical studies. The current study on scalable noble metal free electrode and the performance results forms part of important milestones aimed towards the development of AEMWE and its commercialization prospects.

Experimental Methods

Preparation and Characterization of Self supported catalysts: The catalysts were processed by a simple and scalable approach involving two-step process (**Scheme 1a**). For the processing of the self-supported catalysts, nickel foam (NF) having an initial thickness of 1600 µm (MTI Japan) was treated with 1 M HCl aq. and acetone before drying to remove the residual oxide layer, after mechanically pressed to varying (220–800 µm) thickness. Chloride salt of iron ($FeCl_3$) was used as the metallic precursor (Sigma-Aldrich, USA) and H_2Na_2OP was used as the phosphide precursor (Fujifilm Chemicals, Japan). For the Ni_2P-Fe/NF processing, in the first step 0.3 g $FeCl_3$ was dissolved in 50 ml deionized water before immersing the treated NF and keeping it for ~1.5 h without stirring. Before the second step involving heat treatment to form the desired catalyst, the NF with precursor coating was dried at ambient conditions slightly. To impart phosphorization, the NF with Fe precursor was heated at 350 °C at 3 °C/min ramp rate and held for 4 h in a tubular furnace along with the phosphide precursor at the front end of the furnace having high purity N_2 flowing at 60 SCCM. The heating time was also varied in later study further to identify the effect

of varying phosphorization time on catalyst formation and properties. The overall loading of the catalysts was analyzed by weight change after the different processing conditions.

The initial phase identification of the NF-based catalysts was done using the XRD patterns recorded at a scan rate of 3 °/min using an Ultima IV (Rigaku, Japan) system, with Cu Kα (λ = 1.5406 Å) X-ray source operating at 40 kV and 40 mA. The surface morphological characteristics and elemental distribution of the metal species on the self-supported catalysts before and after electrochemical reactions were documented using SEM (S-8400, Hitachi High Technologies, Japan). XPS analysis (Quantum 2000, ULVAC-PHI Inc., Japan) fitted with a twin-anode X-ray source using Al Kα radiation (hv = 1486.58 eV) was used for confirming the surface elemental composition and identifying oxidation states of the metal species in the nanostructures. The XPS spectra curves obtained were fitted using the Gauss-Lorentz wave shape function and the background was revised using "Shirley". The catalyst compositions in each cases were calculated from inductively coupled plasma - atomic emission spectrometry (ICP-AES) analysis after dissolving the catalyst by using aqua regia.

Electrochemical Studies: For the CV and CA tests using the processed catalysts, electrochemical measurement system using a potentiostat and an electrode rotating system (HZ-7000 and HR-500, Hokuto Denko, Japan) was used. OER studies in alkaline solution were evaluated by CV using a three-electrode system with Hg/HgO and a Pt wire as the reference and counter electrodes, respectively. The NF-based catalysts with active geometrical area of 2 cm_{geo}^2 (*by dipping the desired area of catalyst in the electrolyte and the remaining portion being masked by a Teflon tape*) being used as the working electrode (*can be seen in Fig. S16 and Fig. S17 in the supporting information*). The OER performances were recorded at a scan rate of 10 mV s^{-1} in a N$_2$-saturated 1 M KOH aqueous solution at room temperature. After the initial surface activation using 30 CV cycles between 1.2 and 1.8 V vs

RHE, OER currents were collected from the cathodic CV profiles to eliminate the effect of nickel oxidation on the performance analysis. All potential values in half-cell conditions were converted to RHE according to the equation: $E_{RHE} = E_{Hg/HgO} + 0.917$ V. Ohmic losses were corrected using the measured current (i) and solution resistance (R), which were obtained by ac impedance as follows: iR corrected $E = E_{RHE} - i \cdot R$. The accelerated durability test (ADT) for the OER catalysts was performed at 100 mV s^{-1} scan rate for 1000 cycles in N$_2$-saturated 1 M KOH (aq.). In addition, the chronoamperometry (CA) studies were conducted using constant potential of 1.5 V vs RHE for 12 h in N$_2$-saturated 1 M KOH (aq.).

Anion Exchange Membrane preparation:

To prepare a PE(VBTAC) pore-filling membrane as an AEM, poly (vinyl benzyl trimethyl ammonium chloride) (PVBTAC), which was cross-linked by divinyl benzene, was filled in the pores of a polyethylene (PE) porous substrate (thickness = 25 µm, porosity = 46%, Toray Industries, Inc.) using the impregnation polymerization method reported in our previous study.[61] The thickness the prepared PE(VBTAC) membranes were about 25 µm. This developed membrane is cost-effective, can be easily prepared and is also scalable using the commercially available monomer and the porous polymer substrate.

Preparation and performance evaluation of MEAs for AEMWE:

Slurry preparation for Cathode & Anode Coating of Commercial Catalysts: For preparation of Pt/C slurry, 40 mg of 46.5 wt. % Pt/C (TEC10E50E, Tanaka Kikinzoku Kogyo K.K., Japan) and 13.33 mg of PFT-C6-TMA ionomer (M_w = 178000 g/mol and ion exchange capacity = 3.2 mequiv/g) were dispersed in 5 ml water-IPA mixture (1:1 volume). Here, high molecular weight ionomer with M_w >100,000 was used. Due to the well-entanglement of polymer chains by its high molecular weight, it is stable and does not leach in hot water despite its high IEC.[14] The above

mixture was ball-milled for 1 h at 150 rpm speed using a planetary ball mill (Pulverisette 6, Fritsch, Germany). Similarly, for IrO_2 slurry preparation, 40 mg IrO_2 (Alfa Aesar, USA) and 13.33 mg PFT-C6-TMA ionomer were dispersed in 5 ml of 1:1 volume ratio IPA-water mixture through sonication for 1 h.

MEA fabrication using NF-based catalysts at anode: Prior to the MEA fabrication, a NF-based catalyst (5 cm^2 in area) was immersed in a solution of PFT-C6-TMA (10 mg in 10 ml 1:1 volume ratio IPA-water mixture) for 30 min and then dried for another 30 min at 60 °C. This process allows to form a thin layer of the polymer on the catalyst surface. This polymer layer is necessary for the efficient conduction of OH^- in the three-phase boundary at pure water operation. For the cathode, the prepared Pt/C slurry was coated on the one side of the AEM of a PE(VBTAC) pore-filling membrane using a pulsed spray system (Nordson K.K., Japan). The loading of Pt at the cathode was maintained at 0.3 mg_{Pt}/cm^2. The NF-based catalyst and the cathode-catalyst-coated membrane were assembled in an electrolyzer cell with serpentine flow channels. On the cathode side, carbon paper (SGL 29 AA, SGL Carbon, Germany) was used as a diffusion layer whereas at the anode modified NF itself functions as a diffusion layer. The gasket thickness was adjusted according to NF thickness employed.

MEA fabrication using commercial PGM catalysts at anode & cathode: For comparing the performance of the processed NF catalysts with commercial catalysts, IrO_2 and Pt/C were used as anode and cathode catalysts, respectively. The anode and cathode catalyst layers were prepared using the catalyst-coated membrane technique. In this case, IrO_2 slurry was spray-coated on one side of PE(VBTAC) membrane to be used as the anode electrode. The loading of IrO_2 at the anode was 1.2 mg/cm^2. For the cathode, the prepared Pt/C slurry was coated on the other side of the

PE(VBTAC) pore-filling membrane AEM with the loading of Pt at the cathode being maintained at 0.3 mg$_{Pt}$/cm^2.

Cell testing procedure: To evaluate AEMWE performances of the MEAs using the modified NF-based catalysts, 1 M KOH aqueous solution or pure water was fed to the anode side of the cell. Initially, the MEA was conditioned by applying a current density of 100 mA/cm^2 until the cell voltage became stable. The flow of 1 M KOH aq. was maintained at 5 mL/min and the cell temperature was kept at 80 °C during the conditioning and electrochemical measurements. After conditioning, polarization curves of the cells for AEMWE were recorded using an HJ1010SD8 charge–discharge unit (Hokuto Denko, Japan) followed by the MEA stability tests performed at a current density of 200 mA/cm^2 for ~24 h. The energy conversion efficiency of water electrolysis was calculated using the equation, $thermal\ neutral\ voltage/cell\ operating\ voltage \times 100$, with thermal neutral voltage (1.48 V). Electrochemical impedance spectroscopy (EIS) was measured at a DC voltage of 1.5 V vs RHE with a DC amplitude of 10 mV and was performed by an electrochemical measurement system equipped with an impedance analyzer (HZ-7000, Hokuto Denko, Japan).

Supporting Information

XRD patterns for the catalysts; XPS spectra for the catalysts; OER cyclic voltammetry profiles for the self-supported catalysts; Comparison tables for OER half-cell characteristics and AEMWE performances involving the catalysts processed; Charge density plots for the catalysts during C_{dl} analysis; Electrolyzer performances curves of Ni_2P-Fe/NF anode catalyst with varying electrode thickness in pure water fed condition; SEM micrographs and EDS spectra of catalyst surfaces after durability tests; Images for modified and bare NF; images for the electrochemical set up and during OER and single cell AEMWE; Video of alkaline OER using Ni_2P-Fe/NF (SV-1)

References

1. S. Sherif, F. Barbir, T. Veziroglu, Towards a Hydrogen Economy, *Electr. J.* 18 (**2005**) 62–76. **DOI**: https://doi.org/10.1016/j.tej.2005.06.003

2. M. Dresselhaus, I. Thomas, Alternative energy technologies, *Nature* 414 (**2001**) 332–337. **DOI**: https://doi.org/10.1038/35104599

3. J.A. Turner, Sustainable hydrogen production, *Science* 305 (**2004**) 972–974. **DOI**: https://doi.org/10.1126/science.1103197

4. O. Schmidt, A. Gambhir, I. Staffell, A. Hawkes, J. Nelson, S. Few, Future Cost and Performance of Water Electrolysis: An Expert Elicitation Study, *Int. J. Hydrog. Energy* 42 (**2017**) 30470–30492. **DOI**: https://doi.org/10.1016/j.ijhydene.2017.10.045

5. M. Schalenbach, A.R. Zeradjanin, O. Kasian, S. Cherevko, K.J. Mayrhofer, A Perspective on Low-Temperature Water Electrolysis-Challenges in Alkaline and Acidic Technology, *Int. J. Electrochem. Sci.* 13 (**2018**) 1173–1226. **DOI**: 10.20964/2018.02.26

6. Z. Yana, J. L. Hitta, J. A. Turnerb, T. E. Mallouk, Renewable electricity storage using electrolysis, *PNAS* 117 (**2020**) 12558–12563. **DOI**: https://doi.org/10.1073/pnas.1821686116

7. Z. D. Árpád, B. Palotás, Impact of the current fluctuation on the efficiency of Alkaline Water Electrolysis, *Int. J. Hydrog. Energy* 42 (**2016**) 5649–5656. **DOI**: 10.1016/j.ijhydene.2016.11.142

8. K. Li, S. Yu, D. Li, L. Ding, W. Wang, Z. Xie, E. J. Park, C. Fujimoto, D. A. Cullen, Y. S. Kim, F-Y. Zhang, Engineered Thin Diffusion Layers for Anion-Exchange Membrane

Electrolyzer Cells with Outstanding Performance, *ACS Appl. Mater. Interfaces* 13 (**2021**) 50957−50964. **DOI**: https://doi.org/10.1021/acsami.1c14693

9. Y. S. Kim, Polymer Electrolytes with High Ionic Concentration for Fuel Cells and Electrolyzers, *ACS Appl. Polym. Mater. 3* (**2021**) 1250−1270. **DOI:** https://doi.org/10.1021/acsapm.0c01405

10. C. G. Arges and V. Ramani, Two-dimensional NMR spectroscopy reveals cation-triggered backbone degradation in polysulfone-based anion exchange membranes, *PNAS* 110 (**2013**), 2490-2495. **DOI:** https://doi.org/10.1073/pnas.1217215110

11. S. Miyanishi, T. Yamaguchi, Ether cleavage-triggered degradation of benzyl alkylammonium cations for polyethersulfone anion exchange membranes, *Phys.Chem.Phys.Chem.* 18 (**2016**) 12009-12023. **DOI**: https://doi.org/10.1039/C6CP00579A

12. E.J. Park, Y.S. Kim, Quaternized aryl ether-free polyaromatics for alkaline membrane fuel cells: synthesis, properties, and performance-a topical review, *J. Mater. Chem.* 6, (**2018**),15456-15477. **DOI**: https://doi.org/10.1039/C8TA05428B

13. H.P.R. Graha, S. Ando, S. Miyanishi, T. Yamaguchi, Development of a novel durable aromatic anion exchange membrane using a thermally convertible precursor, *Chem. Commun.* 54 (**2018**) 10820-10823. **DOI**: https://doi.org/10.1039/C8CC05371E

14. S. Miyanishi, T. Yamaguchi, Highly conductive mechanically robust high Mw polyfluorene anion exchange membrane for alkaline fuel cell and water electrolysis application, *Poly. Chem.* 11(**2020**) 3812–3820. **DOI**: https://doi.org/10.1039/D0PY00334D

15. D. Li, E. J. Park, W. Zhu, Q. Shi, Y. Zhou, H. Tian, Y. Lin, A. Serov, B. Zulevi, E. D. Baca, C. Fujimoto, H. T. Chung, Y. S. Kim, Highly quaternized polystyrene ionomers for high performance anion exchange membrane water electrolysers, *Nat. Energy* 5 (**2020**) 378–385. **DOI**: https://doi.org/10.1038/s41560-020-0577-x

16. R. Soni, S. Miyanishi, H. Kuroki, T. Yamaguchi, Pure Water Solid Alkaline Water Electrolyzer Using Fully Aromatic and High-Molecular-Weight Poly(fluorene-*alt*-tetrafluorophenylene)-trimethyl Ammonium Anion Exchange Membranes and Ionomers, *ACS Appl. Energy Mater.* 4, 2, (**2021**) 1053–1058. **DOI**: https://doi.org/10.1021/acsaem.0c01938.s001

17. M. S. Cha, J. E. Park, S. Kim, S-H. Shin, S.H. Yang, S. J. Lee, T-H. Kim, D. M. Yu, S. So, K. M. Oh,Y-E. Sung, Y-H. Cho, J. Y. Lee, Oligomeric chain extender-derived anion conducting membrane materials with poly(pphenylene)- based architecture for fuel cells

and water electrolyzers, *J. Mater. Chem. A*, 10 (**2022**) 9693-9706. **DOI**: https://doi.org/10.1039/D1TA10868A

18. H. A. Miller, K. Bouzek, J. Hnat, S. Loos, C.I Bernacker, T. Weißgarber, L. Rontzsch, J. Meier-Haack, Green hydrogen from anion exchange membrane water electrolysis: a review of recent developments in critical materials and operating conditions, *Sustainable Energy Fuels* **4** (**2020**) 2114-2133. **DOI**: https://doi.org/10.1039/C9SE01240K

19. S.H. Ahn, S. J. Yoo, H-J. Kim, D. Henkensmeier, S W. Nam, S-K. Kim, J. H. Jang, Anion exchange membrane water electrolyzer with an ultra-low loading of Pt-decorated Ni electrocatalyst, *Appl. Catal., B* 180 (**2016**) 674–679. **DOI**: https://doi.org/10.1016/j.apcatb.2015.07.020

20. J. Song, C. Wei, Z-F. Huang, C. Liu, L. Zeng, X. Wang, Z. J. Xu A review on fundamentals for designing oxygen evolution electrocatalysts**,** *Chem. Soc. Rev.***,** 49 (**2020**) 2196-2214. **DOI**: https://doi.org/10.1039/C9CS00607A

21. N. Cheng, S. Stambula, D. Wang, M. N. Banis, J. Liu, A. Riese, B. Xiao, R. Li, T.-K. Sham, L.-M. Liu, G. A. Botton, X. Sun, Platinum single-atom and cluster catalysis of the hydrogen evolution reaction, Nat. *Commun.* 7 (**2016**) 13638. **DOI**: https://doi.org/10.1038/ncomms13638

22. M.S. Faber, S. Jin, Earth-abundant inorganic electrocatalysts and their nanostructures for energy conversion applications, *Energy Environ. Sci.* 7 (**2014**) 3519–3542. **DOI**: https://doi.org/10.1039/C4EE01760A

23. Y. Lee, J. Suntivich, K. J. May, E. E. Perry, Y. Shao-Horn, Synthesis and Activities of Rutile IrO_2 and RuO_2 Nanoparticles for Oxygen Evolution in Acid and Alkaline Solutions, *J. Phys. Chem. Lett.* 3 (**2012**) 399−404. **DOI**: https://doi.org/10.1021/jz2016507

24. D.-H. Park, M.-H. Kim, H.-J. Lee, W.-J. Lee, J.-H. Byeon, J.-H. Kim, J.-S. Jang, K.-W. Park, Development of Ni-Ir Oxide Composites as Oxygen Catalysts for an Anion-Exchange Membrane Water Electrolyzer, *Adv. Mater. Interfaces* **2022,** 2102063. **DOI:** https://doi.org/10.1002/admi.202102063

25. Y. Zhou, S. Xi, X. Yang, H. Wu, In situ hydrothermal growth of metallic Co_9S_8-Ni_3S_2 nanoarrays on nickel foam as bifunctional electrocatalysts for hydrogen and oxygen evolution reactions, *J. Solid State Chem.* 270 (**2019**) 398–406. **DOI:** https://doi.org/10.1016/j.jssc.2018.12.004

26. S. Sankar, Y. Sugawara, S. A. Aravindh, R. Jose, T. Tamaki, G. M. Anilkumar, T. Yamaguchi, Tuning Palladium Nickel Phosphide toward Efficient Oxygen Evolution

Performance, *ACS Appl. Energy Mater.* 3 (**2020**) 879−888. **DOI:**
https://dx.doi.org/10.1021/acsaem.9b01996

27. X. Jia, Y. Zhao, G. Chen, L. Shang, R. Shi, X. Kang, G. I. N. Waterhouse, L.-Z. Wu, C.-H. Tung, T. Zhang, Ni_3FeN Nanoparticles Derived from Ultrathin NiFe-Layered Double Hydroxide Nanosheets: An Efficient Overall Water Splitting Electrocatalyst, *Adv. Energy Mater.* 6 (**2016**) 1502585. **DOI:** https://doi.org/10.1002/aenm.201502585

28. A. Mendoza-Garcia, D. Su, S. Sun, Sea urchin-like cobalt–iron phosphide as an active catalyst for oxygen evolution reaction, *Nanoscale 8* (**2016**) 3244-3247. **DOI:** https://doi.org/10.1039/C5NR08763E

29. A. Han, H. Chen, H. Zhang, Z. Sun, P. Du, Ternary metal phosphide nanosheets as a highly efficient electrocatalyst for water reduction to hydrogen over a wide pH range from 0 to 14, *J. Mater. Chem. A* 4 (**2016**) 10195–10202. **DOI:** https://doi.org/10.1039/C6TA02297A

30. B. Liu, B. He, H. Q. Peng, Y. Zhao, J. Cheng, J. Xia, J. Shen, T. W. Ng, X. Meng, C. S. Lee, W. Zhang, Unconventional Nickel Nitride Enriched with Nitrogen Vacancies as a High-Efficiency Electrocatalyst for Hydrogen Evolution, *Adv. Sci.* 5 (**2018**) 1800406. **DOI:** https://doi.org/10.1002/advs.201800406

31. Y. Shi, B. Zhang, Recent advances in transition metal phosphide nanomaterials: synthesis and applications in hydrogen evolution reaction, *Chem. Soc. Rev.* 45 (**2016**) 1529 -1541. **DOI:** https://doi.org/10.1039/C5CS00434A

32. X. Xiao, L. Tao, M. Li, X. Lv, D. Huang, X. Jiang, H. Pan, M. Wang, Y. Shen, Electronic modulation of transition metal phosphide *via* doping as efficient and pH-universal electrocatalysts for hydrogen evolution reaction, *Chem Sci.* 9 (**2018**) 1970–1975. **DOI:** https://doi.org/10.1039/C7SC04849A

33. N. A. Karim, M. S. Alias, H. Yang, Recent Developments for the Application of 3D Structured Material Nickel Foam and Graphene Foam in Direct Liquid Fuel Cells and Electrolyzers, *Catalysts* **2021**, 11, 279 **DOI:** https://doi.org/10.3390/catal11020279

34. L. Wan, J. Liu, Z. Xu, Q. Xu, M. Pang, P. Wang, B. Wang, Construction of Integrated Electrodes with Transport Highways for Pure-Water-Fed Anion Exchange Membrane Water Electrolysis, *Small* (**2022)** 2200380 (1-11). **DOI:** https://doi.org/10.1002/smll.202200380

35. D. Li, A.R. Motz, C. Bae, C. Fujimoto, G. Yang, F-Y. Zhang, K.E. Ayers, Y.S. Kim, Durability of anion exchange membrane water electrolyzers, *Energy Environ. Sci.*,14 (**2021**) 3393–3419. **DOI:** https://doi.org/10.1039/D0EE04086J

36. C. Andronescu, S. Barwe, E. Ventosa, J. Masa, E. Vasile, B. Konkena, S. Moller, W. Schuhmann, Powder Catalyst Fixation for Post-Electrolysis Structural Characterization of NiFe Layered Double Hydroxide Based Oxygen Evolution Reaction Electrocatalysts *Angew. Chem. Int. Ed.* 56 (**2017**) 11258–11262. **DOI:** https://doi.org/10.1002/anie.201705385

37. Y. Li, H. Zhang, T. Xu, Z. Lu, X. Wu, P. Wan, X. Sun, L. Jiang, Under-Water Superaerophobic Pine-Shaped Pt Nanoarray Electrode for Ultrahigh-Performance Hydrogen Evolution, Adv. *Funct. Mater. 25* (**2015**) 1737–1744. **DOI:** https://doi.org/10.1002/adfm.201404250

38. H. Jin, B. Ruqia, Y. Park, H.J. Kim, H.-S. Oh, S.-I. Choi, K. Lee, Nanocatalyst Design for Long-Term Operation of Proton/Anion Exchange Membrane Water Electrolysis, *Adv. Energy Mater.* 11 (**2021**) 2003188. **DOI:** https://doi.org/10.1002/aenm.202003188

39. Y. Li, H. Zhang, M. Jiang, Q. Zhang, P. He, X. Sun, 3D Self-Supported Fe-Doped Ni_2P Nanosheet Arrays as Bifunctional Catalysts for Overall Water Splitting, *Adv. Funct. Mater.* 27 (**2017**) 1702513. **DOI:** https://doi.org/10.1002/adfm.201702513

40. J. Kwon, H. Han, S. Choi, K. Park, S. Jo, U. Paik, T. Song, Current Status of Self-Supported Catalysts for Robust and Efficient Water Splitting for Commercial Electrolyzer, *ChemCatChem* 11 (**2019**) 5898–5912. **DOI:** https://doi.org/10.1002/cctc.201901638

41. N. K. Chaudhari, H. Jin, B. Kim, K. Lee, Nanostructured materials on 3D nickel foam as electrocatalysts for water splitting, *Nanoscale* 9 (**2017**) 12231–12247. **DOI:** https://doi.org/10.1039/C7NR04187J

42. B. You, N. Jiang, M. Sheng, M. W. Bhushan, Y. Sun, Hierarchically Porous Urchin-Like Ni_2P Superstructures Supported on Nickel Foam as Efficient Bifunctional Electrocatalysts for Overall Water Splitting, *ACS Catal.* 6 (**2016**) 714–721. **DOI:** https://doi.org/10.1021/acscatal.5b02193

43. L-A. Stern, L. Feng, F. Song, X. Hu, Ni_2P as a Janus catalyst for water splitting: the oxygen evolution activity of Ni_2P nanoparticles, *Energy Environ. Sci.*, 8 (**2015**) 2347-2351. **DOI:** https://doi.org/10.1039/C5EE01155H

44. H. Liang, A. N. Gandi, D. H. Anjum, X. Wang, U. Schwingenschlögl, H. N. Alshareef, Plasma-Assisted Synthesis of NiCoP for Efficient Overall Water Splitting, *Nano Lett.* 16 (2016) 7718–7725. **DOI:** https://doi.org/10.1021/acs.nanolett.6b03803

45. P. E. R. Blanchard, A. P. Grosvenor, R. G. Cavell, A. Mar, X-ray Photoelectron and Absorption Spectroscopy of Metal-Rich Phosphides *M*2P and *M*3P (*M)* Cr-Ni), *Chem. Mater.* 20 (**2008)** 7081–7088. **DOI:** https://doi.org/10.1021/cm802123a

46. B. Zhang, Y. H. Lui, L. Zhou, X. Tang, S. Hu, An alkaline electro-activated Fe–Ni phosphide nanoparticle-stack array for high-performance oxygen evolution under alkaline and neutral conditions, *J. Mater. Chem. A* 5 (2017) 13329–13335. **DOI:** https://doi.org/10.1039/C7TA03163G

47. Y. Jia, W. Cai, X. Li, X-Y. Yu, Z. Hong, Fe ions modulated formation of hollow NiFe oxyphosphide spheres with enhanced oxygen evolution performance, *Chem. Commun.* 55 (**2019**) 14371-14374. **DOI:** https://doi.org/10.1039/C9CC07747B

48. H. Q. Fu, L. Zhang, C. W. Wang, L. R. Zheng, P. F. Liu, H.G. Yang, 1D/1D Hierarchical Nickel Sulfide/Phosphide Nanostructures for Electrocatalytic Water Oxidation, *ACS Energy Lett.* 3 (**2018**) 2021–2029. **DOI:** https://doi.org/10.1021/acsenergylett.8b00982.s001

49. M. Qian, S. Cui, D. Jiang, L. Zhang, P. Du, Highly Efficient and Stable Water-Oxidation Electrocatalysis with a Very Low Overpotential using FeNiP Substitutional-Solid-Solution Nanoplate Arrays, *Adv. Mater.* 29 (**2017**) 1704075. **DOI:** https://doi.org/10.1002/adma.201704075

50. R. Ge, S. Wang, J. Su, Y. Dong, Y. Lin, Q. Zhang, L. Chen, Phase-selective synthesis of self-supported RuP films for efficient hydrogen evolution electrocatalysis in alkaline media**,** *Nanoscale* 10 (**2018**) 13930-13935. **DOI:** https://doi.org/10.1039/C8NR03554G

51. A. R.J. Kucernak, K.F. Fahy, V. N. N. Sundaram, Facile synthesis of palladium phosphide electrocatalysts and their activity for the hydrogen oxidation, hydrogen evolutions, oxygen reduction and formic acid oxidation reactions, *Catalysis Today* 262 (**2016**) 48–56. **DOI:** https://doi.org/10.1016/j.cattod.2015.09.031

52. J. J. Kaczur, H. Z. Yang, Z. C. Liu, S. A. Sajjad, R. I. Masel, Carbon dioxide and water electrolysis using new alkaline stable anion membranes, *Front. Chem.* 6, (**2018**) 1-16. **DOI:** https://doi.org/10.3389/fchem.2018.00263

53. Y. J. Leng, G. Chen, A. J. Mendoza, T. B. Tighe, M. A. Hickner, C-Y. Wang, Solid-state water electrolysis with an alkaline membrane , *J. Am. Chem. Soc.* 134 (**2012**) 9054–9057. **DOI:** https://doi.org/10.1021/ja302439z

54. T. Pandiarajan, L. J. Berchmans, S. Ravichandran, Fabrication of spinel ferrite based alkaline anion exchange membrane water electrolysers for hydrogen production. *RSC Adv.* 5 (**2015**) 34100–34108. **DOI:** https://doi.org/10.1039/C5RA01123J

55. A. Alobaid, C. Wang, R. A. Adomatis, Mechanism and Kinetics of HER and OER on NiFe LDH Films in an Alkaline Electrolyte, *J. Electrochem. Soc.,* 165 (15) (**2018**) J3395-J3404. **DOI:** https://doi.org/10.1149/2.0481815jes

56. M.W. Louie, A.T. Bell, An Investigation of Thin-Film Ni–Fe Oxide Catalysts for the Electrochemical Evolution of Oxygen, *J. Am. Chem. Soc.* 135 (**2013**) 12329–12337. **DOI:** https://doi.org/10.1021/ja405351s

57. I. Vincent, D. Bessarabov, Low-cost hydrogen production by anion exchange membrane electrolysis: a review, *Renew. Sustain. Energy Rev*. 81 (**2018**) 1690–1704. **DOI:** https://doi.org/10.1016/j.rser.2017.05.258

58. L. Trotochaud, S. L. Young, J. K. Ranney, S. W. Boettcher, Nickel-iron oxyhydroxide oxygen-evolution electrocatalysts: the role of intentional and incidental iron incorporation. *J. Am. Chem. Soc.*, 136 (**2014**) 6744-6753. **DOI:** https://doi.org/10.1021/ja502379c

59. H. Zhang, A. W. Maijenburg, X. Li, S. L. Schweizer, R. B. Wehrspohn, Bifunctional Heterostructured Transition Metal Phosphides for Efficient Electrochemical Water Splitting, *Adv. Funct. Mater.* 30 (**2020**) 2003261. **DOI:** https://doi.org/10.1002/adfm.202003261

60. K. Liu, F. Wang, P. He T.A. Shifa, Z. Wang, Z. Cheng, X. Zhan, J. He, The Role of Active Oxide Species for Electrochemical Water Oxidation on the Surface of 3d-Metal Phosphides, *Adv. Energy Mater.* 8 (**2018**) 1703290. **DOI:** https://doi.org/10.1002/aenm.201703290

61. G. S. Sailaja, S. Miyanishi, T. Yamaguchi, A durable anion conducting membrane with packed anion-exchange sites and an aromatic backbone for solid-state alkaline fuel cells, *Polym. Chem.*, 6 (**2015**) 7964-7973. **DOI:** https://doi.org/10.1039/C5PY01058F